Chemical Systems and Reactivity

1. Fundamentals of supramolecular chemistry

Host-guest chemistry

Nature of Supramolecular Interactions

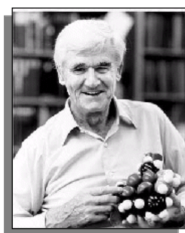**Porphyrins and tetrapyrrole macrocycles**

Supramolecular features of Plant Photosynthesis

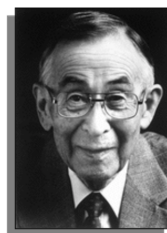**Crown ethers**

Spherands

Cryptands

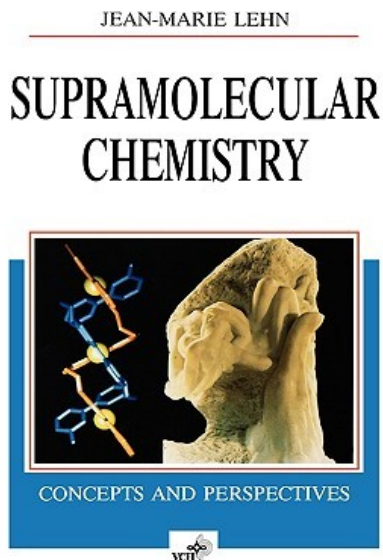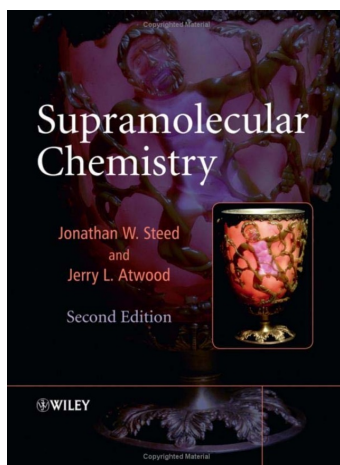**Calixarenes**

| Donald J. Cram | Jean-Marie Lehn | Charles J. Pedersen |

Nobel Prize in Chemistry 1987.

"Supramolecular chemistry is the chemistry of the intermolecular bond, covering the structures and functions of the entities formed by the association of two or more chemical species" (J. M. Lehn).

Supramolecular Chemistry. Jonathan W. Steed, Jerry L. Atwood. John-Wiley&Sons, 2000.

Supramolecular Chemistry: Concepts and Perspectives,, J.-M. Lehn, Wiley-VCH (1995) ISBN 978-3527293117

Host-guest chemistry

Supramolecular chemistry: host-guest chemistry

The host

Large molecule or aggregate possessing a sizeable central hole or cavity. Supramolecular chemistry is closely related to the synthesis of macrocyclic structures.

The guest

An ionic species, a simple molecule or a more sophisticated species such as an hormone or neurotransmitter
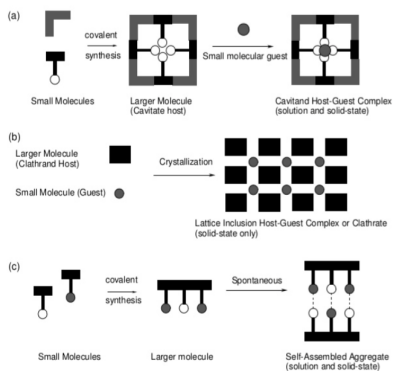
The host-guest complex

Figure 1: Illustration of the difference between a cavitate and a clathrate by inclusion of the guest in the cavity of the host (Adapted from Steed&Atwood

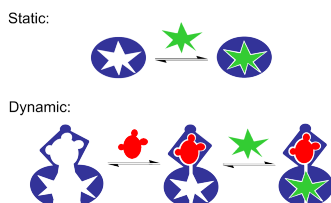Molecular recognition driven by non-covalent interactions

Figure 2: Illustration of the formation of a host-guest complex by non-covalent interactions and key-and-lock mechanism. (Adapted from Wikipedia).

Replication and self-organisation; Adaptative evolution dynamics controlled by the environment.
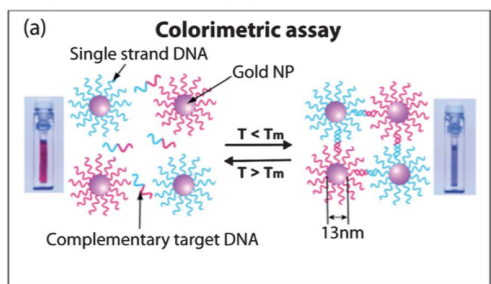

Figure 3: Self-assembled nanomaterials for diagnostics and sensing. (a) Colorimetric detection of single stranded DNA by hybridization with gold nanoparticles decorated with complementary single stranded DNA. The resulting aggregates, which display very sharp melting transitions, are easily observed by a visible color change or by UV-Vis spectroscopy. (Adapted from Eric Busseron et al, Nanoscale, 2013, 5, 7098).

https://www.youtube.com/watch?v=sP7H61BhgdQ

Table 1: Host-guest complexes of neutral hosts

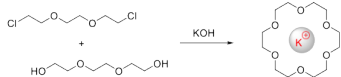| Host	Guest	Interaction	Example
Crown-ether	Metal cation	Ion-dipole	$[K^+\text{-}[18]crown\text{-}6]$
Spherand(Sph)	$[NH_3]$	HB	$Sph\text{-}[NH_3]$
Calixarene	Organic molecule	Dispersion	$Calix[4]arene\text{-}toluene$
Water clathrate	Organic molecule	Dispersion	$[H_2O]_6\text{-}CH_4$

Crown-ethers

Figure 4: Synthesis of a macro-cyclic by using potassium ion as the template cation (Adapted from Steed&Atwood).
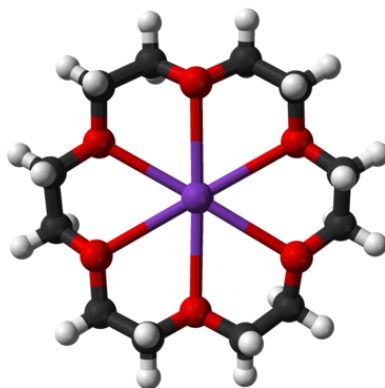

Figure 5: 18-crown-6 ether coordinating a potassium ion (Adapted from Steed &Atwood).

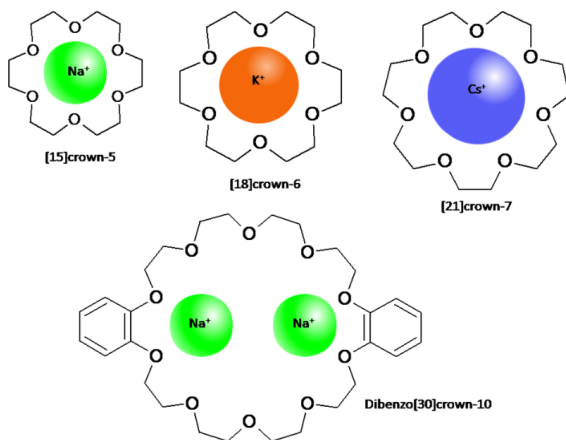Figure 6: Size complementarity principle for crown ethers. Adapted from J. M. Lehn, Supramolecular Chemistry: Concepts and Perspectives, VCH, Weinheim, 1995.
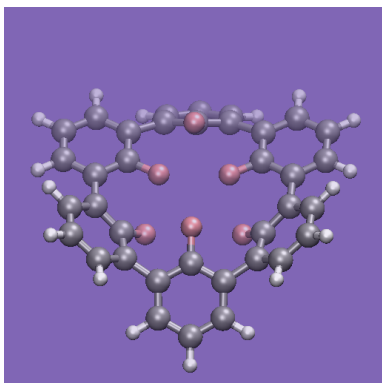
Spherands/Cryptands

Figure 7: Fluorinated spherand macrocycle (BJCC, unpublished).
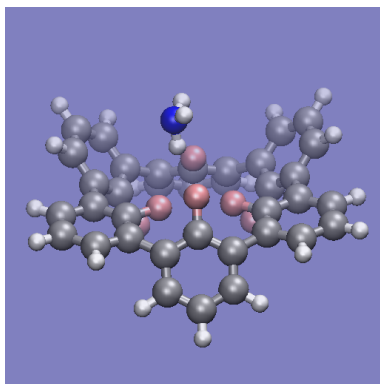

Figure 8: Complex of a fluorinated spherand with an ammonia molecule (BJCC, unpublished).

Calixarenes
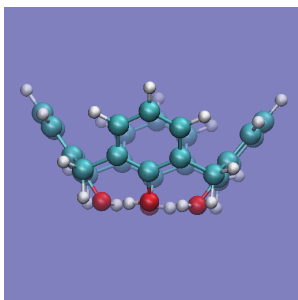
Figure 9: Cone calix[4]arene. From Bernardino&BJCC, Supramolecular Chemistry (2002).
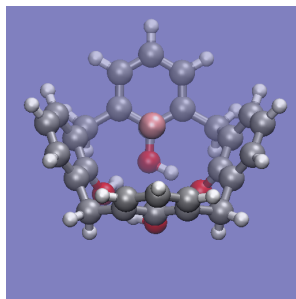
Figure 10: Cone calix[4]arene conformer: complex with a K+ cation.

Curcubits

Figure 11: Curcubit[4]-uril. From Iqmol database.
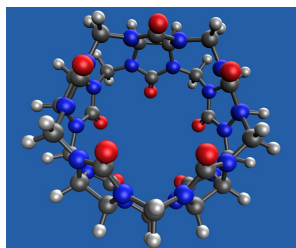
Figure 12: Curcubit[5]-uril. From Iqmol database.

Water clathrates
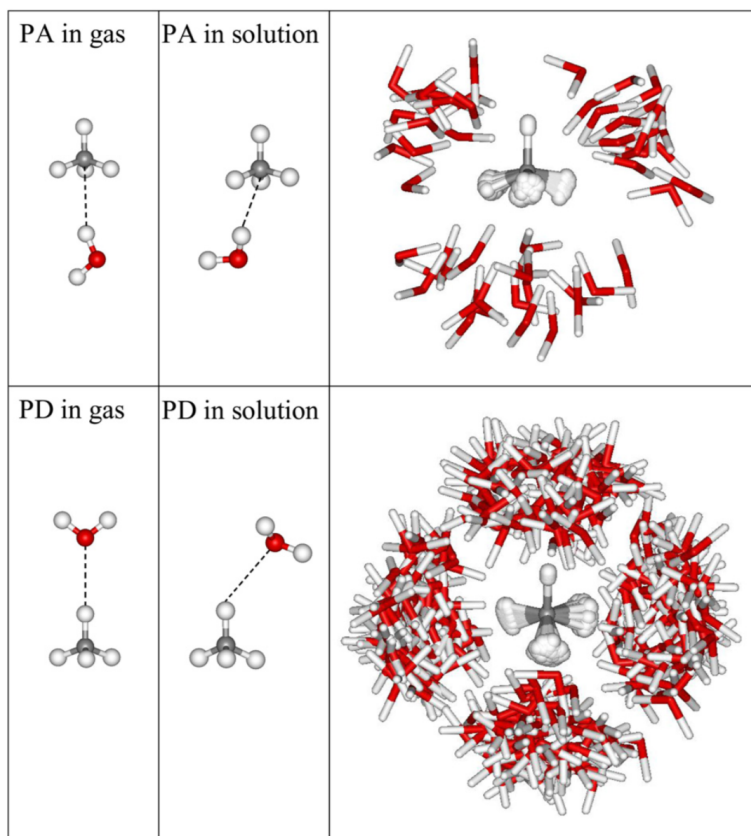
Figure 13: Illlustration of the CH_4-water interactions, which define the confinement of CH_4 in water clathrates. From M. Mateus et al, Chemical Physics Letters, v 506, 183, 2011.

Nature of Supramolecular Interactions

Traditional chemistry focuses on the covalent bond. Supramolecular chemistry mainly involves weaker and non-covalent interactions between molecules.
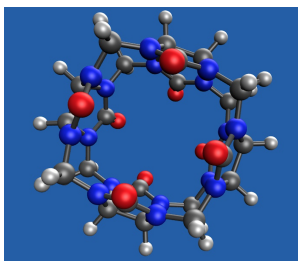
Table 2: Non-covalent driving interactions in supramolecular chemistry

Type	Strength (kJ/mol)
ion-ion	$\sim 100 - 350$
ion-dipole	$\sim 50 - 200$
dipole-dipole	$5 - 50$
Hydrogen bond	$4 - 120$
Cation$-\pi$	$5 - 80$
Dispersion (vdw)	< 5
$\pi - \pi$ stacking (vdw)	$0 - 50$

Ion-Ion interactions
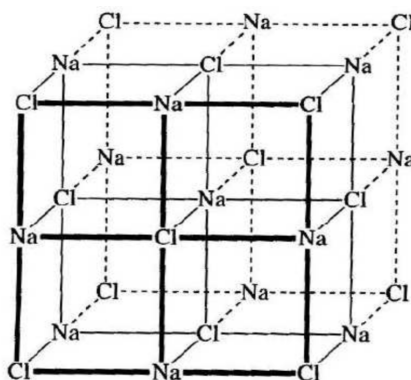
Figure 14: NaCl ionic lattice (Adapted from Steed &Atwood).

Ion-dipole interactions

Figure 15: Ion-dipole interactions (Adapted from Steed &Atwood).

Hydrogen bonding in calixarene

Figure 16: Hydrogen bonding in the calix[4]arene lower rim. From Bernardino&BJCC,Supramolecular Chemistry, v14, 57, 2002).

Dispersion (vdw) interactions
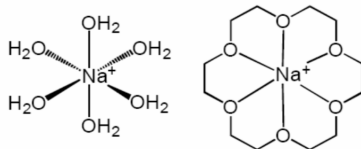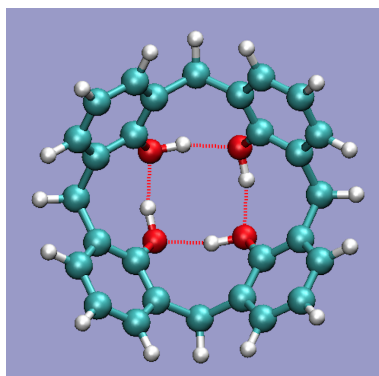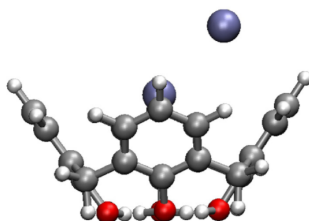

Figure 17: Complex of calix[4]arene with Ar_2. From BJCC et al, Chemical Physics Letters, v612, 266, 2014.

Porphyrins and tetrapyrrole macrocycles

Tetrapyrrole macrocycles

Macrocycles with large internal ring with size-selective binding to ionic metallic species. Extensive redox chemistry associated with the reduction of the conjugated ring framework.

Main features

The (near) planar ring is energetically stable although some geometric distortions are observed when they interact with an environment. This stability is related to the presence of a conjugated π system. This macrocycle is an aromatic system containing 22 π-electrons. However only 18 of them are delocalized according to the Huckel's rule of aromaticity: $4n+2$ delocalized π-electrons, where $n = 4$ (see figure below).

Figure 18: Conjugation in free-base porphyrin: the path in red follows alternating single and double bonds. There are 9 double bonds along the red path and 18 π electrons.

The macrocycles are highly selective with regard to the ionic radius of the metal ion they will bind
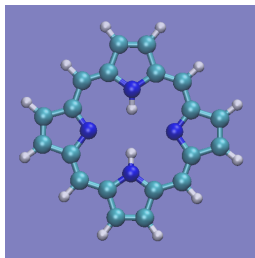
Figure 19: Free-base porphyrin.
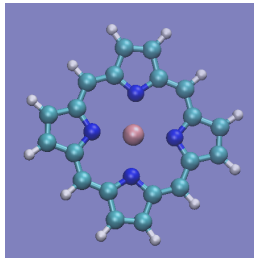
Figure 20: Mg-porphyrin.

Exercise The electronic spectrum of free base porphyrin can be discussed by using Huckel theory. For cyclic conjugated systems, the energy levels are given by

$$\epsilon_k = \alpha + 2\beta cos(\frac{2k\pi}{N})$$ (1)

where, N is the number of π electrons, $k = 0, \pm 1, \pm 2, ..., \pm N$. α and β are parameters, that are usually named coulomb integral and bond integral, respectively.

a) suppose that α can be taken as zero, and that benzene absorbs at 260 nm with a transition energy of 2β. Calculate β.

b) By using the value of β of the previous item, estimate the first transition energy of free base porphyrin.
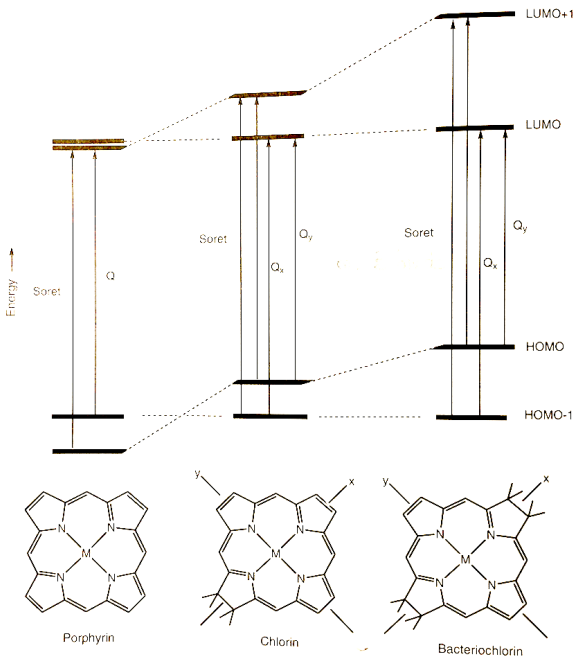
Figure 21: Simplified molecular orbital energy levels of porphyrin, chlorin, and bacteriochlorin. From R. E. Blankenship, Molecular mechanisms of Photosynthesis (Blackwell 2002).

Figure 22: Monomers and dimers of phthalocyanine. From BJCC et, Chem. Phys. Lett (2014)

Figure 23: Spectra of phtalocyanine monomers and dimers.

Figure 24: Low energy spectra of phtalocyanine monomers and dimers.

Heat-induced formation of one-dimensional coordination polymers on Au(111): an STM study†

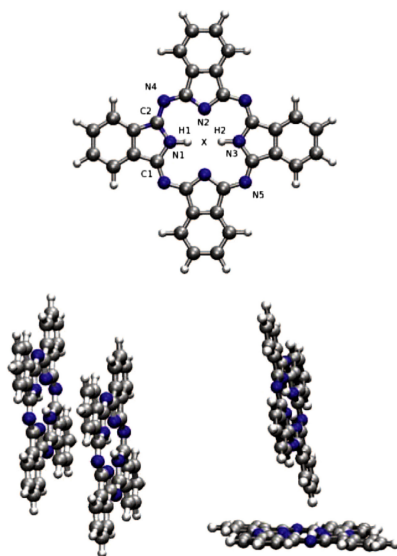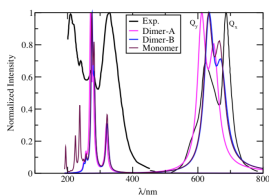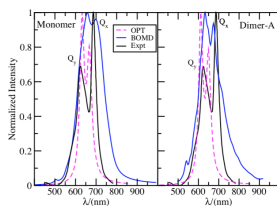Tuan Anh Pham,*[a] Fei Song,[a] Mariza N. Alberti,[b] Manh-Thuong Nguyen,[c] Nils Trapp,[b] Carlo Thilgen,[b] François Diederich[b] and Meike Stöhr*[a]
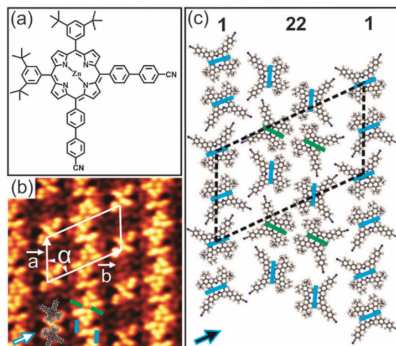
Fig. 1 (a) Chemical structure of porphyrin **1**. (b) Close-up STM image (15 × 15 nm², $U = -1.8$ V, $I = 20$ pA) showing the 2D close-packed pattern for close to 1 ML coverage. (c) Tentative model for the molecular network. The unit cell vectors **a** and **b** are denoted by white arrows in (b). The blue and green bars in (b) represent two different conformational isomers of **1**. The arrows in (b) and (c) indicate one of the three principal directions of the substrate.
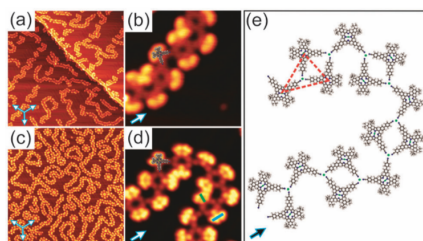
Fig. 2 (a and c) Overview STM images (150 × 150 nm²), showing the formation of 1D coordination polymers of **1** on Au(111) induced by annealing at 160 °C and deposition of Co, respectively. The set of three arrows indicates the principal directions of the underlying substrate. (b and d) Close-up STM images (15 × 15 nm²) for (a) and (c), respectively. Blue and green bars in (d) indicate A and B isomers, respectively. (e) The proposed model for the 1D coordination polymer of **1** on Au(111). The green dots in (e) represent Au atoms, while the red dashed triangle illustrates a basic unit of the 1D polymer. The STM images were taken at 77 K with $U = -1.8$ V, $I = 20$ pA.

Supramolecular features of plant photosynthesis

Macrocycles with a labile Mg^{2+} cation play a fundamental role as energy harvesters in photosynthesis, a process by which organic matter is produced from CO_2 and water.

$$H_2O + CO_2 \xrightarrow{\text{Photosynthesis}} 1/n(CH_2O)_n + {}^3O_2, \quad \Delta H = 470 \text{kJ/mol} \quad (2)$$
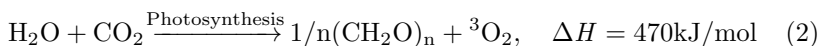
Photosynthesis is carried out by green plants, some bacteria, and algae. Oxidation can involve water as wells as other substrates such as H_2S. Efficient photosynthesis relies on the presence of a number of different light harvest systems pigments (chromophores). These pigments are all based on tetrapyrolle macrocycles and include several different species of **chlorophyll and bacteriochlorophylls**.
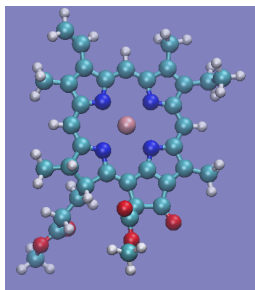
Figure 25: chlorophyll a
Aliphatic phytil chain not shown.
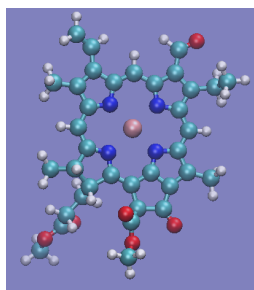
Figure 26: chlorophyll b
Aliphatic phytil chain not shown.
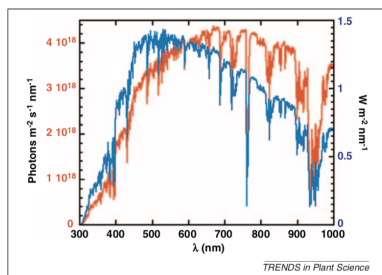
Figure 27: Standard reference solar spectrum used to evaluate solar cells and photosynthetic efficiency, which can be downloaded at http://rredc.nrel.gov/solar/spectra/am1.5/. The blue curve is the energy output spectrum and the red curve is the photon flux spectrum. The photon flux spectrum is more relevant for a quantum energy storage process such as photosynthesis.
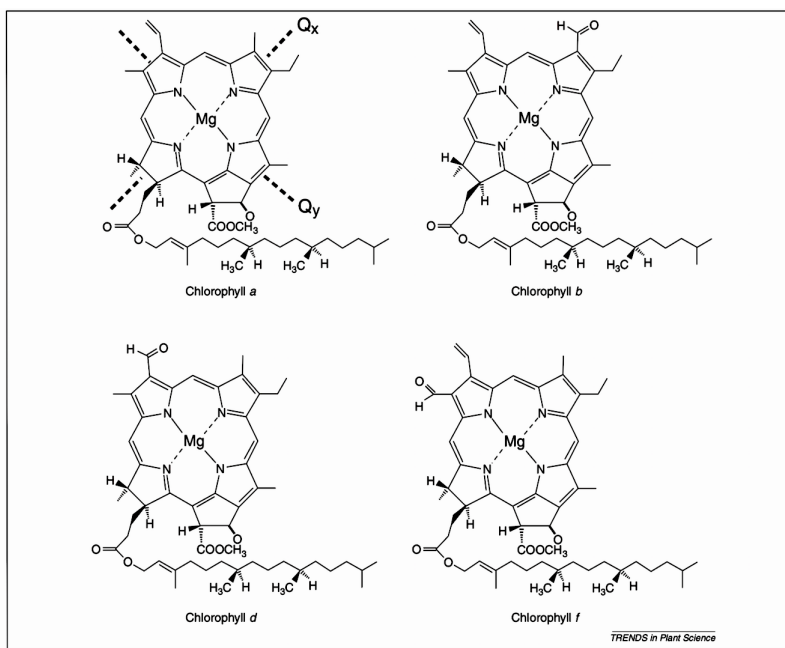
Figure 28: Chemical structures of chl a, b, d, and f. From M. Shen and R. E. Blankenship.Trends in Plant Science (2011).
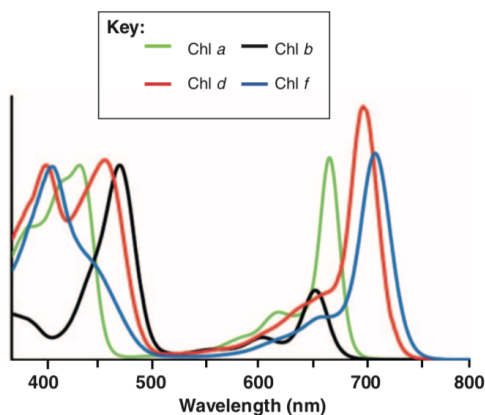
Figure 29: Absorption spectra of chl a, b, d, and f. From M. Shen and R. E. Blankenship.Trends in Plant Science (2011).

Exercise: The intensity of full sunlight in the photosynthetically active radiation (PAR) window is estimated as $\sim 1800\mu E$ m^{-2} s^{-1}, where the Einstein E unit is by definition $1E \equiv$ the energy of one mole of photons. The photon flux I is defined as $I = E \times N_A$, which can be calculated as $I = 1.1 \times 10^{21}$ photons m^{-2} s^{-1}.

a) Assume that a chlorophyll molecule is roughly square with dimension of ~ 10 Å per side. Estimate I in Å^{-2} s^{-1}.

b) Suppose that the effective target σ associated with one chlorophyll molecule is proportional to the strength of the absorption intensity, which is given by the Beer-Lambert law ($A = \epsilon cl$), where A is the absorbance, c the concentration, and ϵ the molar extinction coefficient. We will write $\sigma \sim 2.303\epsilon$, where the factor 2.303 comes from converting from natural logs to base 10 logs. By taking an average value for ϵ as 25×10^3 M^{-1} cm^{-1} or $\epsilon = 25 \times 10^6$ cm$^2 \times N_A^{-1}$, show that $\sigma = 0.96$ Å^2.

c) The number of hits per molecules or absorbed photons per molecule can be calculated as $I \times \sigma \sim 10$. Justify.
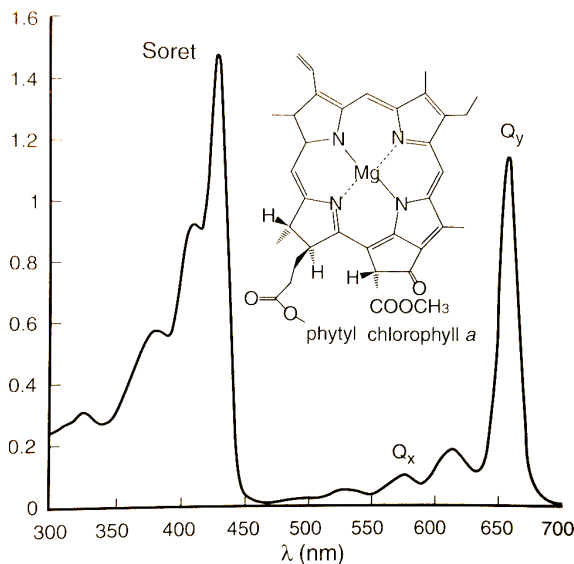
Figure 30: Absorption spetrum of chla illustrating the (high energy) Soret and (low energy) Q bands. From R.E. Blankenship, Molecular Mechanisms of Photosynthesis.
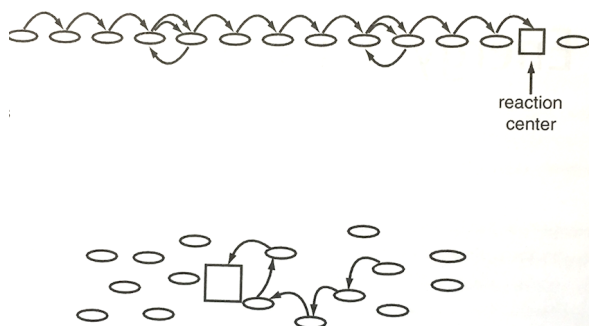
Figure 31: Excitation propagation in one- and three dimensional antenna models. From R.E. Blankenship, Molecular Mechanisms of Photosynthesis.

The funnel concept in photosynthesis: sequential excitations of higher energy pigments transfer energy to lower excite lower energy excitations and deliver these energies to the reaction center.
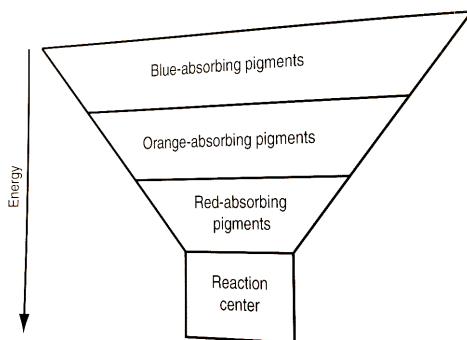
Figure 32: Funnel concept in photosynthetic antennas illustrating the participation of different pigments. From R. E. Blankenship. Molecular Mechanisms of Photosynthesis.
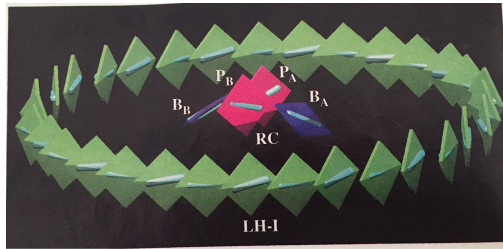
Figure 33: Simplified representation of the light harvesting system I (LHI). Bacteriochlorophylls (BChls) are represented by squares. Antennas in green, special pair in red, accessories BChls in blue. The special pair, the accessories BChls integrate the reaction center. From X. Hu and K. Schulten, Physics Today (1997).

Crown ethers, spherands, and cryptands

Thermodynamic and Kinetic selectivity

The affinity of a host H for a specific guest G can be discussed by using the following relation between the respective concentrations

$$\text{Host} + \text{Guest} \rightleftharpoons \text{Host.Guest} \tag{3}$$

which leads to the definition of a binding constant K

$$K = \frac{[\text{Host.Guest}]}{[\text{Host}] \times [\text{Guest}]} \tag{4}$$

We can also define the selectivity of one guest relative to another by:

$$\text{Selectivity} = \frac{K_{\text{Guest1}}}{K_{\text{Guest2}}} \tag{5}$$

The thermodynamic stability of metal(M)-macrocycle(L) in a given solvent (often water and methanol) can be described by

$$M[H_2O]_n^{m+} + L \rightleftharpoons ML^{m+} + nH_2O \tag{6}$$
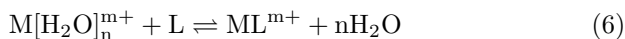
which leads to the following expression for K

$$K = \frac{[ML^{m+}]}{[(M(H_2O)_n)^{m+}] \times [L]}, \qquad (\text{units} : M^{-1}) \tag{7}$$

A large binding constant K is associated with a high concentration of a bound metal and a more stable metal-macrocycle complex.

Typical values of K: for crown ethers and alkali metals in water $K \in [10^1 - 10^2]$. In methanol this value increases up to 10^6 for the $[K^+ \subset [18]\text{crown-6}]$. For the K^+-[2.2.2]cryptand complex K is $\sim 10^{10}$.

In sequential processes involving the binding of two metallic species to a macrocycle, two values of K can be measured: K_{11} and K_{12}.

$$M[H_2O]_n^{m+} + L \overset{K_{11}}{\rightleftharpoons} ML^{m+} + nH_2O \tag{8}$$

$$M[H_2O]_n^{m+} + ML^{m+} \overset{K_{12}}{\rightleftharpoons} M_2L^{2m+} + nH_2O \tag{9}$$
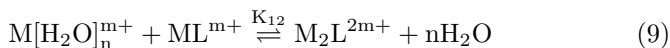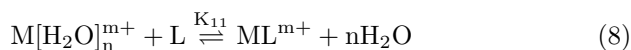
where

$$K_{12} = \frac{[M_2L^{2m+}]}{[M(H_2O)_n^{m+}] \times [ML^{m+}]} \tag{10}$$

In these cases, a two-binding constant can be defined as

$$\beta_{12} = K_{11} \times K_{12} \tag{11}$$

Considering the widely variation of binding constants, it is more convenient to define

$$\log\beta_{12} = \log K_{11} \times K_{12} = \log K_{11} + \log K_{12} \tag{12}$$

The binding constant K is related to the free energy through the Gibbs equation

$$\Delta G^o = -RT\ln K \tag{13}$$

and therefore the affinity of a host to a guest can be given in terms of K or ΔG^o.

Selectivity of cation complexation

The selectivity of a given host for a particular cation involves the determination of the thermodynamic binding constant for a reference system (e.g. K^+) and the ratio relative to other species.

Some specific features contributing to the binding constant

- size match between cation and host cavity

- electrostatic potential (charge)

- solvent polarity, hydrogen bonding and coordination

- degree of host preorganisation

- enthalpic and entropic contribution to the cation-host interactions

- cation and host free energies of solvation

Crown ethers

Ubiquitous macrocycles in supramolecular chemistry with specific affinity to cations and neutral molecules. Their structure is defined by a cyclic array of oxygen atoms linked by organic spacers such -CH_2CH_2- groups.

Discovered by Charles Pedersen (1987 Nobel Prize)
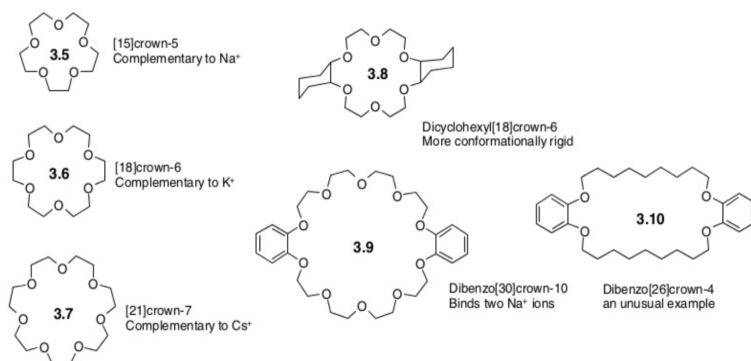
Figure 34: Some common crown ethers. From Steed&Atwood.
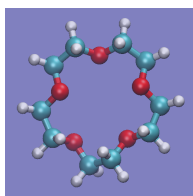
Figure 35: 15-crown-5.
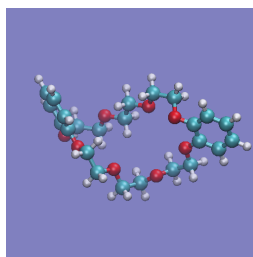
Figure 36: dibenzo-24-crown-8

Table 3: Diameters of different crown ethers vs ionic radii of several metal cations (Adapted from Steed&Atwood).

Cation	Diameter /Å	Crown ether	Cavity dimension /Å
Li^+	1.36	12-crown-4	$1.20 - 1.50$
Na^+	1.90	15-crown-5	$1.70 - 2.20$
K^+	2.66	18-crown-6	$2.60 - 3.20$
Cs^+	3.38	21-crown-7	$3.40 - 4.30$
Cu^+	1.92		$1.20 - 1.50$
Ag^+	2.52		$1.20 - 1.50$
Mg^{2+}	1.44		$1.20 - 1.50$
Ca^{2+}	2.20		$1.20 - 1.50$
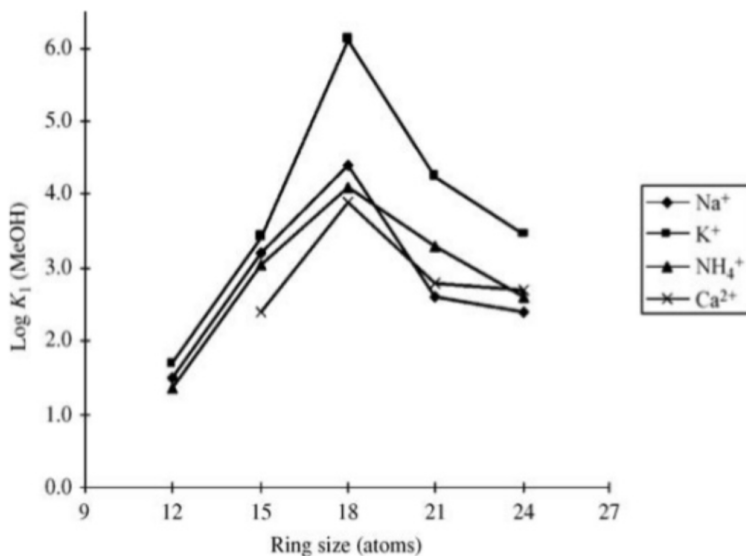
Figure 37: Dependence of K_1 on the crown ether ring size. From Steed&Atwood.

Spherands

Donald Cram (Nobel Prize 1987)

Main interest: design of a relatively rigid host in solution characterised by the presence of a central binding pocket fostering strong binding and selectivity among cations.
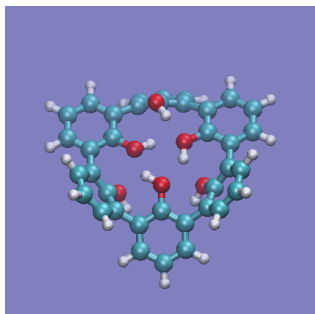
Figure 38: Spherand-OH.
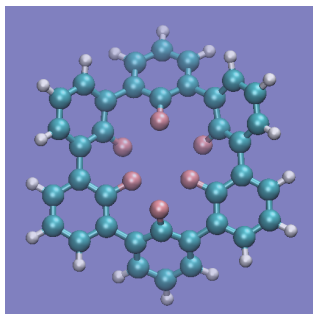
Figure 39: Spherand-F

The spherand-OH macrocycle shows a strong affinity for small cationic species (Li^+, Na^+). However, there are some indications that the spherand-F substituted structure exhibits no clear selectivity for cationic species. Citing Steed&Atwood: "Apparently, the intrinsic affinity of fluoro substituents for alkali metal cations is so low that even the incorporation of multiple binding sites into a highly organised host cannot bring the binding on to a measurable scale."
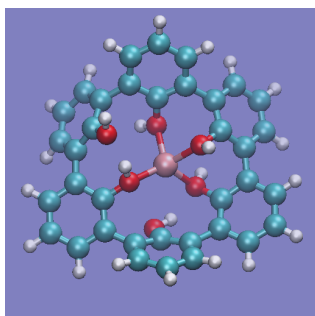
Figure 40: Spherand-OH-Li^+.
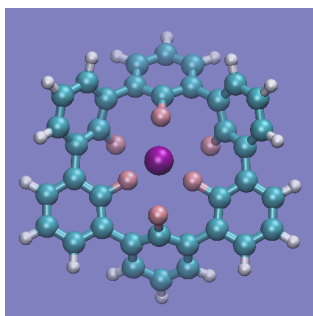
Figure 41: Spherand-F-Na^+.

Cryptands

Jean-Marie Lehn (Nobel Prize 1987)

Design of three-dimensional analogues of crown ethers. The name cryptand is related to their ability to encapsulate a metal cation in a "crypt". The convention for the names of cryptands and some examples are presented below.

l = 1, 2, 3
m = 1, 2, 3
n = 1, 2, 3

l.m.n-crypt

Figure 42

[1.1.1] [2.1.1] [2.2.1] [2.2.2]

[3.2.1] [3.3.2] [3.3.3]
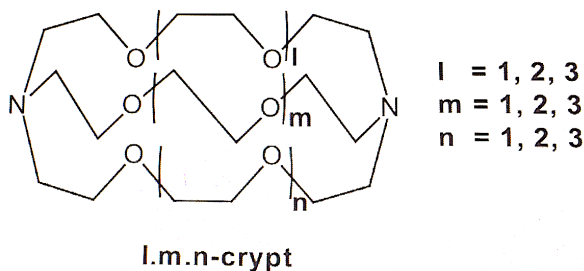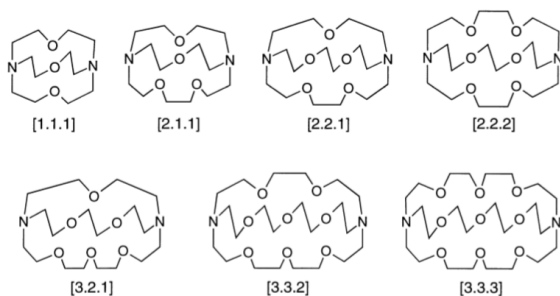
Figure 43: Cryptands (adapted from X.X. Zhang et al., Coordination Chemistry Reviews 174 (1998) 179.)
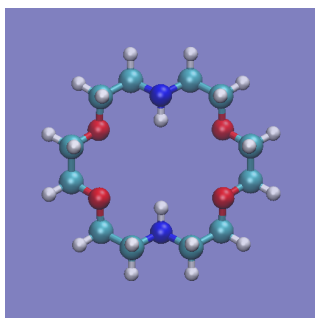
Figure 44: [2.0.2.]-cryptand.
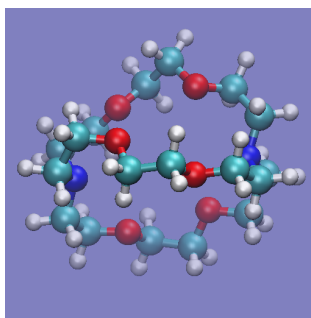
Figure 45: [2.2.2]-cryptand.
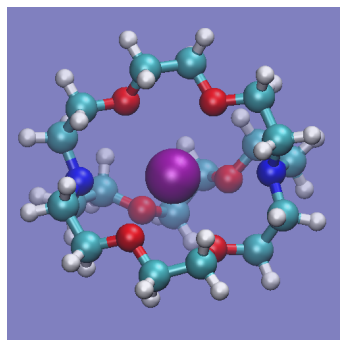
Figure 46: [2.2.2]-cryptand-K$^+$.

The three-dimensional cavity of the cryptands lead to relatively rigid structures in solution. The thermodynamic stabilities of the cryptate complexes is very dependent on the match of the cation size and cryptand cavity diameters.

Table 4: Log K values for the interactions of cryptands with metal ions (Adapted from X.X. Zhang et al., Coordination Chemistry Reviews 174 (1998) 179). Values in Å for the radii of cryptand cavities and ions in parentheses.

	Li^+ (0.68)	Na^+ (0.95)	K^+ (1.33)	Rb^+ (1.48)	Cs^+ (1.69)	Mg^{2+} (0.66)
[1.1.1] (~ 0.5)	1.7	0.8	-	-	-	-
[2.1.1] (0.8)	5.5	3.2	< 2	< 2	< 2	2.5
[2.2.1] (1.1)	2.5	5.4	3.95	2.6	< 2	< 2
[2.2.2] (1.4)	1.25	3.9	5.4	4.35	< 2	< 2
[3.2.2] (2.1)	-	3.2	6.0	6.15	> 6	-
[3.3.3] (2.4)	-	2.7	5.4	5.7	5.9	-
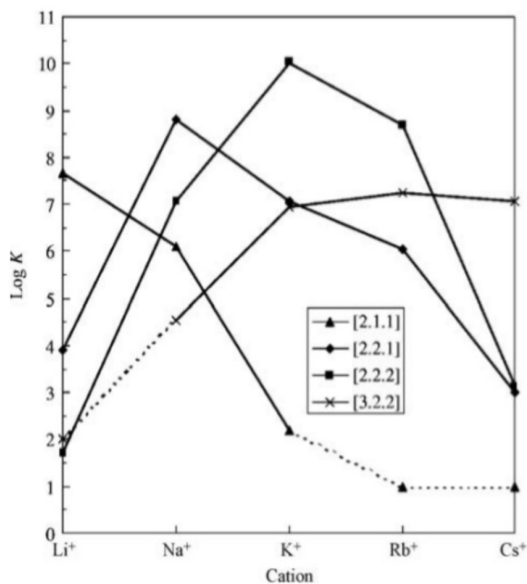
Figure 47: Binding constants for different cryptands in methanol. From Steed&Atwood.

Calix[n]arenes

Class of versatile compounds defined by [n] bridged aromatic rings. The name was proposed by David Gutsche due to the resemblance of the cone conformer with a calix (see Figure below).

Figure 48: Illustration of the similarity between the structure of a calixarene and a calix. From Steed&Atwood.

Depending on their specific functionalisation calix[n]arenes macrocycles can host cationic, anionic, and neutral species.
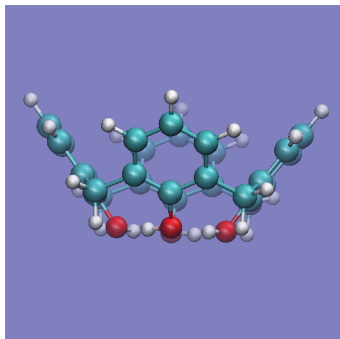
Figure 49: Calix[4]arene (side view).
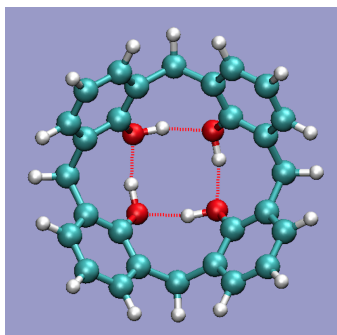
Figure 50: Calix[4]arene (top view).

It is important to stress the different roles played by the upper, middle, and lower rims of calix[n]arenes. These regions define different possibilities of functionalisation and complexation. Of particular interest is the π-electron rich cavity, which size is [n] dependent. This cavity is able to define strong non-covalent dispersion interactions due to electronic cooperativity of the π-electron system.
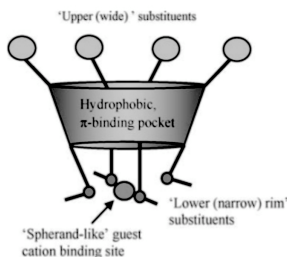
Figure 51: Upper, middle (hydrophobic pocket), and lower rim of calix[4]arene (from Steed&Atwood).

An interesting class of substituted calix[4]arene compounds is defined by the thiacalix[4]arenes, where a sulphur atom (S) replaces the CH_2 group as a link between phenolic moieties.
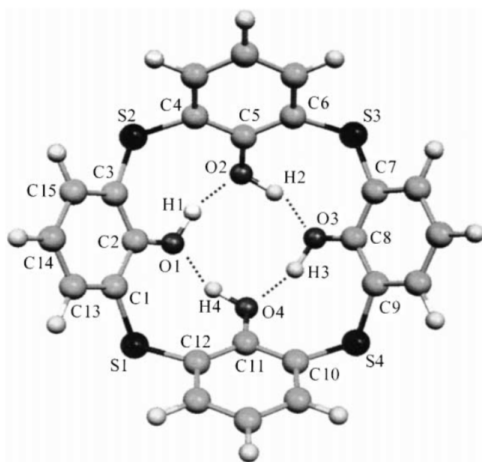
Figure 52: Cone conformer of thiacalix[4]arene. From R.J. Bernardino&BJCC, Theochem (2001).

Conformational equilibrium (structural and energetic aspects).

Calix[n]arenes are characterised by a conformational dynamics at the picosecond scale. The cone conformer is the more energetically stable, although the differences between the cone and other conformers is very dependent on their interactions with the environment and substituent effects.
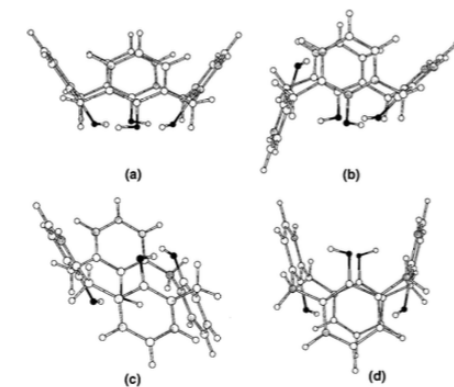
Figure 53: Calix[4]arene conformers. a) cone; b) partial cone; c) 1,2-alternate; d) 1,3-alternate. From R.J. Bernardino, BJCC, JPCA (1999).

Table 2
Total energies (in a.u.) for the thiacalix[4]arene cone conformer. Energy differences (ΔE's in kcal/mol) between the conformers (partial-cone, 1,2-alternate and 1,3-alternate) and the cone conformer

|	Cone	ΔE		
	Total	Partial-cone	1,2-Alternate	1,3-Alternate
Thiacalix[4]arene				
HF/3-21G[a]	−2793.12214	22.1	33.7	30.8
HF/3-21G(d,p)[a]	−2793.67636	19.4	29.9	27.8
B3LYP/3-21G[a]	−2803.30453	24.6	44.5	36.1
B3LYP/3-21G(d,p)[a]	−2803.84605	21.3	30.9	31.9
B3LYP/6-31G(d,p)[a]	−2817.88206	10.1	16.5	13.8
B3LYP/6-311G(d,p)[b]	−2818.26308	9.1	15.6	12.3
G96LYP/6-311G(d,p)[b]	−2817.75063	8.2	13.9	11.5
Calix[4]arene				
B3LYP/6-31G(d,p)[c]		10.5	18.3	17.7
Experiment[d]		14.9;13.8		

[a] Geometry optimised at this level of the theory.
[b] Geometry optimised at B3LYP/6-31G(d,p).
[c] Result for calix[4]arene from Bernardino et al. [31].
[d] Free energies of activation $\Delta G^{\ddagger}$ in a solvent (chloroform and benzene, respectively) from Gutsche et al. [32].

The electrostatic potential (again and again)

A fundamental property for discussing complexation of calix[n]arenes with cationic species through cation$-\pi$ interactions is the electrostatic potential. This is illustrated in the figures below.
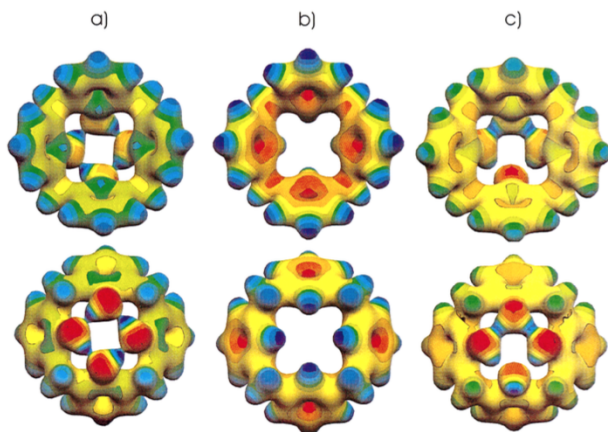
Figure 54: Electrostatic potential over isodensity electronic surfaces. a) cone conformer; b) OH-depleted cone conformer; c) protonated cone. The color coding is the following: red corresponds to the minimum (negative) potential and blue to the maximum (positive) potential. From R.J. Bernardino&BJCC, JPCA (1999).

Cation−π interactions.

The interactions between cations and calix[n]arenes can be of very different nature depending on the binding modes for the complexes. The figure below illustrates two binding modes for Na$^+$-PhOH complex. In the first binding mode (a), a conventional electrostatic interaction between the cation and the oxygen atom explains the energetic stability of the complex. In the second case, the cation is in interaction with the π-electron distribution of the phenol ring and this binding mode is stabilised by cation−π interactions, which are increased by collective additive effects in the cavity of the macrocycles and then become competitive with the exo-type complexation through the lower rim.
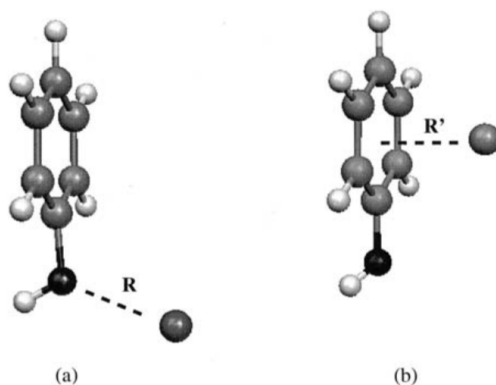
Figure 55: Binding modes for complexes of a cation with a phenolic moiety. From R.J. Bernardino&BJCC, Supramolecular Chemistry (2002).

Cation−π interactions in calix[n]arenes

There is a strong interest in understanding the role played by these interaction in the case of calix[n]arenes. The first relevant aspect concerns the endo- versus exo- complexation, which is determined by a competition between cation−π and electrostatic interactions. Other aspects concern the matching-size between the cation and the cavity, which is of general interest for explaining selectivity and exclusion/inclusion processes.

Figure 56: Complexes of calix[4]arene with different cations (From R.J. Bernardino&BJCC, Supramolecular Chemistry (2002).
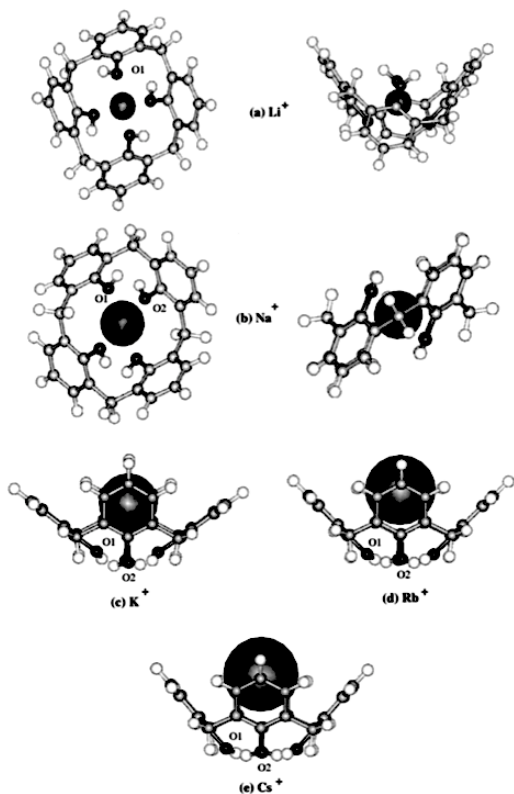
TABLE III Total energies E (in a.u) for the four calix[4]arene conformers represented by X = C (cone), X = PC (partial-cone), X = 1, 2 − A (1,2-alternate), and X = 1, 3 − A (1,3-alternate). ΔE (in kcal/mol) is the complexation energy corresponding to the process $[X–A^+] \rightarrow X+A^+$, where A = H^+, Li^+−Cs^+ Values in parentheses are energy differences (in kcal/mol) relative to the cone conformer

	E	ΔE^*			
	X	X–H^+	X–Li^+	X–Na^+	X–K^+
HF/3-21G†					
C	−1366.17550	−231.7 (0)	−94.5 (0)	−64.5 (0)	−44.9 (0)
PC	−1366.14623	−225.9 (5.8)	−102.7 (−8.2)	−77.5 (−13)	−39.3 (5.6)
1,2-A	−1366.12777	−244.4 (−12.7)	−113.7 (−19.2)	−88.6 (−24)	−40.2 (4.7)
1,3-A	−1366.12452	−216.6 (15.1)	−122.6 (−28.1)	−90.3 (−25.8)	−41.4 (3.5)
HF/6-31G‡					
C	−1373.26269	−226.7 (0)	−83.3 (0)	−51.9 (0)	−35.2 (0)
PC	−1373.24417	−217.6 (11.6)	−86.0 (9.1)	−58.6 (−6.7)	−34.3 (0.9)
1,2-A	−1373.22925	−233.3 (−6.6)	−92.2 (−8.9)	−62.7 (−10.8)	−27.1 (8.1)
1,3-A	−1373.22585	−213.9 (12.8)	−97.5 (−14.2)	−62.9 (−11)	−27.7 (7.5)
HF/3-21G(d,p) †					
C	−1366.33534	−235.7 (0)	−98.7 (0)	−72.4 (0)	−60.5 (0)
PC	−1366.30982	−229.4 (6.3)	−101.9 (−3.2)	−86.1 (−13.7)	−54.1 (6.4)
1,2-A	−1366.29348	−244.7 (−9)	−111.6 (−12.9)	−96.7 (−24.3)	−57.0 (3.5)
1,3-A	−1366.29052	−221.2 (14.5)	−119.6 (−20.9)	−100.1 (−27.7)	−60.7 (−0.2)
HF/6-31G(d,p) ¶					
C	−1373.81606	−222.5 (0)	−75.1 (0)	−45.6 (0)	−38.8 (0)
PC	−1373.80507	−210.3 (12.2)	−74.2 (0.9)	−53.3 (−7.7)	−31.8 (6.5)
1,2-A	−1373.79263	−223.2 (−0.7)	−80.8 (−5.3)	−56.2 (−10.6)	−22.4 (16.4)
1,3-A	−1373.79437	−213.7 (8.8)	−82.6 (−7.5)	−54.3 (−8.7)	−24.4 (14.4)
HF/6-311G(d,p) ¶					
C	−1374.07443	−220.7 (0)	−73.5 (0)	−44.5 (0)	−33.8 (0)
PC	−1374.06510	−208.4 (12.3)	−72.1 (1.4)	−50.5 (−6)	−28.1 (5.7)
1,2-A	−1374.05331	−220.4 (0)	−77.1 (−3.6)	−51.9 (−7.4)	−18.3 (15.5)
1,3-A	−1374.05414	−212.2 (8.5)	−79.6 (−6.1)	−50.0 (−5.5)	−20.8 (13)
MP2/6-31G(d,p) ¶					
C	−1378.26626	−221.4 (0)	−73.8 (0)	−33.4 (0)	–
PC	−1378.25121	−209.4 (12)	−76.5 (−2.7)	−51.9 (−18.5)	–
1,2-A	−1378.23608	−225.5 (−4.1)	−89.1 (−15.3)	−58.5 (−25.1)	–
1,3-A	−1378.23897	−214.7 (6.7)	−91.6 (−17.8)	−58.9 (−25.5)	–
B3LYP/6-31G(d,p) ¶					
C	−1382.40441	−222.0 (0)	−70.8 (0)	−37.9 (0)	−36.6 (0)
PC	−1382.38654	−209.1 (12.9)	−77.4 (−6.6)	−51.4 (−13.5)	−27.5 (9.1)
1,2-A	−1382.37305	−226.5 (−4.5)	−86.0 (−15.2)	−59.3 (−21.4)	−21.0 (15.6)
1,3-A	−1382.36888	−219.3 (2.7)	−92.1 (−21.3)	−63.6 (−25.7)	−29.9 (6.7)

* ΔEs (in kcal/mol) based on single-point HF/D95V calculations with effective core potentials for complexes with cone calyx[4]arene are: −31.7 (K^+); −28.7 (Rb^+); −25.5 (Cs^+). † Optimized geometry at this level of the theory. ‡ Single-point calculation with the HF/3-21G geometry. ¶ Single-point calculation with the HF/3-21G(d,p) geometry.

Figure 57: Data for the binding energies of cations with different conformers of calix[4]arene. From R.J. Bernardino&BJCC, Supramolecular Chemistry (2002).

Electrostatic potential and cation$-\pi$ interactions.

The analysis of the role played by electrostatic potential and cation$-\pi$ interactions should be carried out in a self-consistent way. Actually, the electrostatic potential of the (isolated) host is modified by the presence of the guest, thus leading to a process where the final distribution of the electrostatic potential reflects some intrinsic features of the host as well as the interactions with the guest.
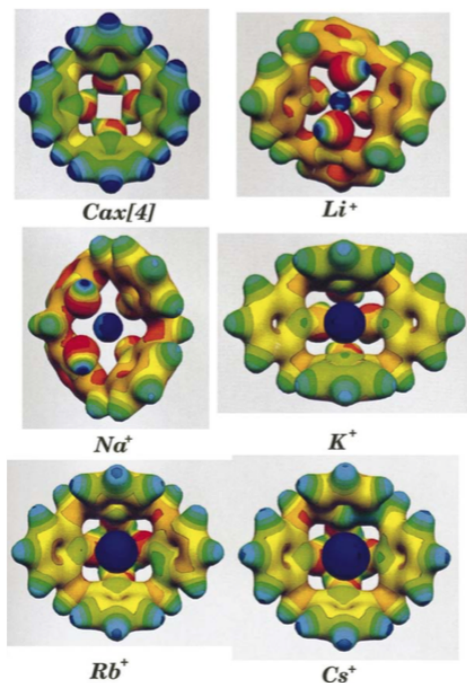

Figure 58: Electrostatic potential over isodensity electronic surfaces for complexes of calix[4]arene with different cations. The color coding is the following: red corresponds to the minimum (negative) potential and blue to the maximum (positive) potential. From R.J. Bernardino&BJCC, Supramolecular Chemistry (2002).

Complexation with neutral species: the role of dispersion

The endo- complexation of neutral species with calix[4]arene is strongly dependent on the correct description of dispersion interactions, quadrupole-quadrupole, and quadrupole-π interactions.
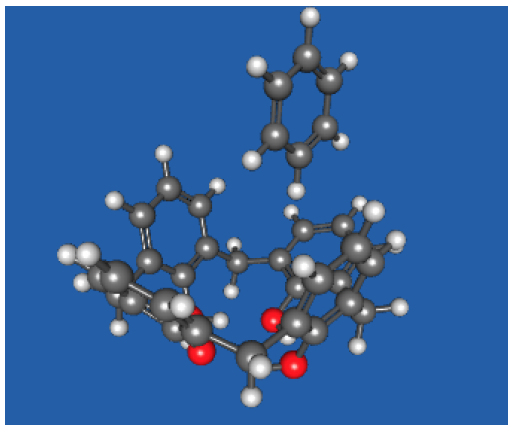

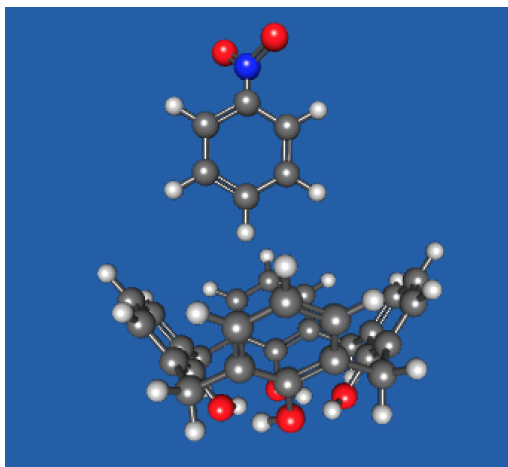Figure 59: Complex of calix[4]arene with benzene.

Figure 60: Complex of calix[4]arene with nitrobenzene.

Complexation of calix[4]arenes with anions: the importance of (lower rim) functionalization.

In contrast with the interactions with cations, calix[n]arene macrocycles need to be modified for making strong interactions with anions. The possibilities are however almost unlimited. One of them is to exploit functionalization of the lower rim by attaching new structures with a favourable interaction with anions. As an example, urea and thiourea substituted calix[4]arenes were proposed as hosts for several small ionic species including F^-, Cl^-, Br^-.
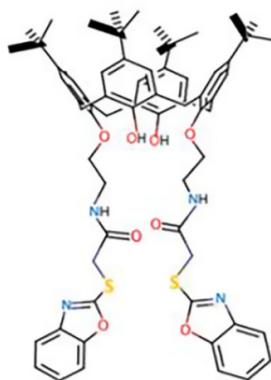

Figure 61: Substituted calix[4]arene illustrating the presence of a thiourea group in the lower rim. Adapted from M. Athar et al., Chemical Physics (2018).
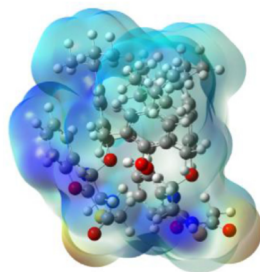

Figure 62: Electrostatic potential for the substituted calix[4]arene (blue region is positive). Adapted from M. Athar et al., Chemical Physics (2018).

Table 4
Interaction energies of three series of the complexes computed at B97D/6-31+G* level of theory. Total binding energies (ΔE_T), the binding energies corrected by BSSE (ΔE_{BSSE}), the binding energies that corrected by BSSE and ZPE (ΔE_{bind}).

System	1			2			3		
	ΔE_T	ΔE_{BSSE}	ΔE_{bind}	ΔE_T	ΔE_{BSSE}	ΔE_{bind}	ΔE_T	ΔE_{BSSE}	ΔE_{bind}
F-	−60.958	−57.482	−57.644	−89.544	−85.512	−83.963	−63.856	−66.106	−62.540
Cl-	−36.290	−35.808	−35.635	−54.183	−53.530	−53.356	−41.234	−41.355	−40.515
Br-	−47.702	−32.673	−32.504	−67.323	−48.417	−47.750	−19.599	−38.756	−18.825
N₃-	−38.235	−36.078	−34.898	−52.316	−49.899	−48.905	−39.062	−40.495	−38.523
SCN-	−32.682	−31.209	−29.862	−47.169	−45.576	−44.475	−32.825	−34.402	−33.161
CN-	−36.268	20.689	21.440	−54.406	−52.681	−51.896	−36.085	−36.376	−34.607

Energies are represented in kcal/mol, BSSE are the basis set superposition error corrected energies (in kcal/mol). ΔZPE, ΔET, are the differences in the zero-point energy and total energy between the product(s) and reactant(s) respectively.

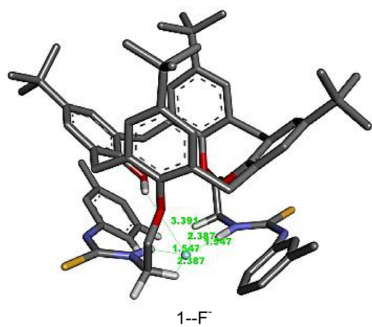Figure 63: Adapted from M. Athar et al., Chemical Physics (2018).

Figure 64: Inclusion of F⁻ in the functionalised lower rim of substituted calix[4]arene. Adapted from M. Athar et al., Chemical Physics (2018).
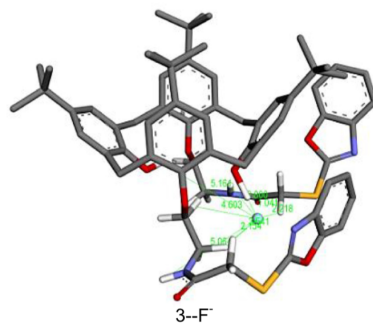

Figure 65: Inclusion of F⁻ in the functionalised lower rim of substituted calix[4]arene. Adapted from M. Athar et al., Chemical Physics (2018).

Weak anion-π interactions in heteroaromatic calix[n]arene receptors.

The design of new macrocycles for anion complexation was also exploited by investigating the interactions with heteroaromatic calix[n]arenes with several anionic species. See figure below for an example of an heteroaromatic macrocycle.
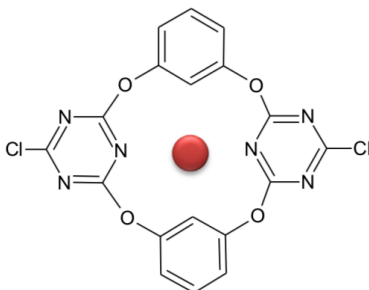

Figure 66: Structure of dichloro-substituted tetraoxacalix[2]arene [2]triazine. From G. Mazzoni et al, Inorganica Chimica Acta (2018).
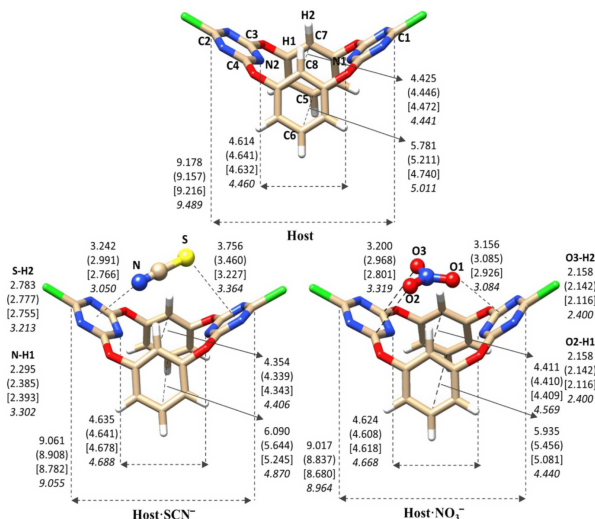

Figure 67: Complexes of tetraoxacalix[2]arene[2]triazine with linear triangular nitrate [SCN]$^-$, and triangular nitrate [NO$_3$]$^-$. Adapted from G. Mazzoni et al, Inorganica Chimica Acta (2018).

Energetics of anion binding to heterocalix[n]arenes.

Table 1
BSSE corrected binding energy (kJ mol^{-1}) computed at 298.15 K.

	Host·SCN$^-$	Host·NO$_3^-$	Host·BF$_4^-$	Host·PF$_6^-$
wB97XD	−15.3	−16.7	−18.3	−6.0
B3LYP-D3	−10.0	−15.7	−16.3	−15.6
RIMP2	−39.9	−39.6	−26.6	−9.5
exp[a]	−13.6	−24.1	−16.1	−14.1

[a] Experimental values have been taken from Ref. [29].

Figure 68: From G. Mazzoni et al, Inorganica Chimica Acta (2018).